AD

CONTRACT REPORT ARBRL-CR-00456

AFATL-TR-81-53

A PRELIMINARY MODEL FOR LOADS ON A PENETRATOR IMPACTING CONCRETE

Prepared by

Orlando Technology, Incorporated
P. O. Box 855
Shalimar, Florida 32579

Technical Monitors

Dr. John A. Zukas, BRL
Mr. John Collins, AFATL

US ARMY ARMAMENT RESEARCH AND DEVELOPMENT COMMAND
BALLISTIC RESEARCH LABORATORY
ABERDEEN PROVING GROUND, MARYLAND

June 1981

Destroy this report when it is no longer needed.
Do not return it to the originator.

Secondary distribution of this report by originating or sponsoring activity is prohibited.

Additional copies of this report may be obtained from the National Technical Information Service, U.S. Department of Commerce, Springfield, Virginia 22161.

The findings in this report are not to be construed as an official Department of the Army position, unless so designated by other authorized documents.

The use of trade names or manufacturers' names in this report does not constitute indorsement of any commercial product.

UNCLASSIFIED

SECURITY CLASSIFICATION OF THIS PAGE *(When Data Entered)*

REPORT DOCUMENTATION PAGE

READ INSTRUCTIONS BEFORE COMPLETING FORM

1. REPORT NUMBER: CONTRACT REPORT ARBRL-CR-00456	2. GOVT ACCESSION NO.
3. RECIPIENT'S CATALOG NUMBER	
4. TITLE *(and Subtitle)*: A PRELIMINARY MODEL FOR LOADS ON A PENETRATOR IMPACTING CONCRETE	5. TYPE OF REPORT & PERIOD COVERED: Technical Report, 1 July 1980-1 February 1981
	6. PERFORMING ORG. REPORT NUMBER
7. AUTHOR(s): John J. Osborn	8. CONTRACT OR GRANT NUMBER(s): DAAK11-79-C-0106
9. PERFORMING ORGANIZATION NAME AND ADDRESS: Orlando Technology, Incorporated, PO Box 855, Shalimar, Florida 32579	10. PROGRAM ELEMENT, PROJECT, TASK AREA & WORK UNIT NUMBERS
11. CONTROLLING OFFICE NAME AND ADDRESS: US Army Armament Research and Development Command, US Army Ballistic Research Laboratory, ATTN: DRDAR-BL, Aberdeen Proving Ground, MD 21005	12. REPORT DATE: JUNE 1981
	13. NUMBER OF PAGES: 37
14. MONITORING AGENCY NAME & ADDRESS *(If different from Controlling Office)*	15. SECURITY CLASS. *(of this report)*: UNCLASSIFIED
	15a. DECLASSIFICATION/DOWNGRADING SCHEDULE

16. DISTRIBUTION STATEMENT *(of this Report)*

Approved for public release; distribution unlimited.

17. DISTRIBUTION STATEMENT *(of the abstract entered in Block 20, if different from Report)*

18. SUPPLEMENTARY NOTES

AFATL-TR-81-53

19. KEY WORDS *(Continue on reverse side if necessary and identify by block number)*

Concrete	Loading Modelling
Penetration	Concrete Impact
Applied Loads	Dynamic Loads

20. ABSTRACT *(Continue on reverse side if necessary and identify by block number)*

The research described in this report was designed to determine analytic equations providing loads on a penetrator element when the penetrator impacts semi-infinite concrete at velocities to 500 m/s. It is assumed that the penetrator's trajectory is controlled with the application of all relevant forces to each penetrator element in a terradynamics computer code.

DD FORM 1 JAN 73 1473 EDITION OF 1 NOV 65 IS OBSOLETE

UNCLASSIFIED

SECURITY CLASSIFICATION OF THIS PAGE *(When Data Entered)*

The loading equations developed in this effort strictly apply only to two-dimensional plane or axisymmetric impacts since they were developed from hydrocode calculations of such situations. Drag coefficients and simplified trajectory equations are developed from the loading equations.

PREFACE

The calculations and analyses in this report were performed by Orlando Technology, Incorporated, P.O. Box 855, Shalimar, Florida 32579, under contract DAAK11-79-C-0106 with the U.S. Army Ballistic Research Laboratory (BRL), Aberdeen Proving Ground, Maryland. The effort was technically monitored by Dr. John Zukas of the BRL and Mr. John Collins of the Air Force Armament Laboratory (AFATL). The AFATL provided funds for portions of this contract.

TABLE OF CONTENTS

LIST OF FIGURES

LIST OF TABLES

SECTION I
SUMMARY

The purpose of this phase of the Ballistic Research Laboratory contract was investigation of the feasibility of developing a simple analytical model which could be used to predict loads on a penetrator in semi-infinite concrete. In its ultimate application this loading model would be applied to penetrator elements in simplified terradynamics computer codes.

A number of calculations were performed using various penetrator, and penetrator element, geometries and velocities in finite difference wave propagation computer codes (hydrocodes). Loads, in terms of applied stresses, were saved from these calculations. They were analyzed to develop equations capable of predicting the applied stress levels as functions of the penetrator's geometry and velocity. It was determined that loading functions could be developed for the relatively simple two-dimensional geometries considered. These functions are presented in this report along with recommendations for extending the analysis to three-dimensional situations and finite thickness targets.

Drag coefficients were developed from the loading functions for relatively simple geometric shapes. These drag coefficients are functions of the reciprocal of the velocity, so that there exists a maximum depth of penetration (i.e., a depth beyond which the penetrator cannot advance). The drag coefficients are applied to a blunt penetrator and comparisons made between a trajectory prediction using them and the trajectory from a hydrocode calculation.

SECTION II
PRELIMINARY CONSIDERATIONS

The concrete material behavior model employed for all hydrocode calculations discussed in this report is presented in detail in Reference 1. The model basically consists of a hydrostat and a yield surface.

The hydrostat defines a relationship between pressure and density and is valid for a good quality concrete with an unconfined compressive yield strength of 5,000 PSI. The hydrostat loading curves, up to 60 kilobars (kb), are defined by the following equations:

$$P = 144\mu \quad \text{if} \quad 0 \leq \mu \leq 0.0025$$

$$P = 0.358 + 78.62\ (\mu - 0.0025) \quad \text{if} \quad 0.0025 < \mu \leq 0.1$$

$$P = 8.0 + 130.0\ (\mu - 0.1) \quad \text{if} \quad 0.1 < \mu \leq 0.2$$

$$P = 21.0 + 420.0\ (\mu - 0.2) \quad \text{if} \quad 0.2 < \mu < 0.3$$

In these equations, P is given in kb and μ is the excess compression defined by:

$$\mu = \rho/\rho_o - 1$$

where ρ_o is ambient concrete density (2.2 g/cc) and ρ is the density at some compressed state.

The yield surface was developed from test data for concretes with varying unconfined compressive strengths and is a function of pressure and the unconfined strength. The yield strength is specified by the following equations:

$$Y = 3\ (P + 0.1f'_c/3)/1.1 \quad \text{if} \quad -0.1\ f'_c/3 \leq P \leq f'_c/3$$

$$Y = P + 2/3f'_c \quad \text{if} \quad f'_c/3 < P \leq 30f'_c$$

$$Y = 30.67f'_c \quad \text{if} \quad 30f'_c < P$$

In these equations f'_c is the unconfined compressive strength of the concrete. The yield surface is a Mohr-Coulomb type with a saturation level set at $30.67f'_c$ (153,000 PSI for a 5,000 PSI concrete).

This concrete model has been successfully employed in penetration and breaching calculations and is actively used at the Air Force Armament Laboratory, the Air Force Weapons Laboratory, the Army Ballistic Research Laboratory and other locations. The model is used in HULL, TOODY, EPIC and other codes with the following constitutive relations.

Deviatoric stresses, ${}^{d}\tau^{ij}$, are computed from deviatoric strains, ${}^{d}\varepsilon^{ij}$, by using the shear modulus, G.

$$ {}^{d}\tau^{ij} = 2\,G\,{}^{d}\varepsilon^{ij} $$

These deviatoric stresses are limited by the yield surface according to the following equation (in two-dimensional geometry)

$$ J_2' = ({}^{d}\tau^{11})^2 + ({}^{d}\tau^{22})^2 + ({}^{d}\tau^{12})^2 + ({}^{d}\tau^{11})({}^{d}\tau^{22}) \leq Y^2/3 $$

where J_2' is the second invariant of the stress deviator tensor. If J_2' exceeds $Y^2/3$, all deviatoric stresses are reset to lie on the yield surface. When the deviatoric stresses have been reset (if necessary) they are added to the pressure to compute the total stress as follows:

$$ \tau^{ii} = {}^{d}\tau^{ii} - P $$

$$ \tau^{ij} = {}^{d}\tau^{ij}, \quad i \neq j $$

This formulation assumes that pressure is positive in compression while stress is negative in compression.

In addition to these equations deviatoric strains and stresses must satisfy the following relationships:

$$ \Delta \equiv \text{dilatation} = -(\varepsilon^{11} + \varepsilon^{22} + \varepsilon^{33}) $$

$$ {}^{d}\varepsilon^{ii} = \varepsilon^{ii} + \Delta/3 $$

$$ {}^{d}\varepsilon^{ij} = \varepsilon^{ij}, \quad i \neq j $$

$$ {}^{d}\varepsilon^{11} + {}^{d}\varepsilon^{22} + {}^{d}\varepsilon^{33} = 0 $$

$$ P \equiv -1/3\,(\tau^{11} + \tau^{22} + \tau^{33}) $$

$$ {}^{d}\tau^{ii} = \tau^{ii} + P $$

$$ {}^{d}\tau^{ij} = \tau^{ij}, \quad i \neq j $$

$$ {}^{d}\tau^{11} + {}^{d}\tau^{22} + {}^{d}\tau^{33} = 0 $$

In one-dimensional plane loading, the strains satisfy the following relationships:

$$\varepsilon^{11} \neq 0$$
$$\varepsilon^{22} = \varepsilon^{33} = 0$$
$$\varepsilon^{12} = \varepsilon^{23} = \varepsilon^{13} = 0$$

where the direction of loading is the "1" direction. This means that the deviatoric strains satisfy the equations:

$$d_{\varepsilon}{}^{11} + 2^{d}\varepsilon^{22} = 0$$
$$d_{\varepsilon}{}^{22} = d_{\varepsilon}{}^{33} = -\tfrac{1}{2}d_{\varepsilon}{}^{11}$$

Since deviatoric stresses are proportional to deviatoric strains, the deviatoric stresses must be related to each other in the same manner as the strains.

$$d_{\tau}{}^{22} = d_{\tau}{}^{33} = -\tfrac{1}{2}d_{\tau}{}^{11}$$

These relations can be put into the yield surface equation for plastic flow to obtain

$$(d_{\tau}{}^{11})^2 + (-\tfrac{1}{2}d_{\tau}{}^{11})^2 + (d_{\tau}{}^{11})(-\tfrac{1}{2}d_{\tau}{}^{11}) = Y^2/3$$

or

$$d_{\tau}{}^{11} = -(2/3)Y$$

where the minus sign indicates compressive flow. Therefore

$$d_{\tau}{}^{22} = d_{\tau}{}^{33} = Y/3$$

and the total stresses in plastic flow then must be

$$\tau^{11} = -(2/3)\ Y-P$$
$$\tau^{22} = \tau^{33} = Y/3 - P$$

From the concrete yield surface equations, P is approximately Y, so the total stresses can be written as

$$\tau^{11} = -(2/3)P - P = -1.67P$$
$$\tau^{22} = \tau^{33} = P/3 - P = -0.67P$$

The ratio of stresses, then, in the loading direction to stresses in the other two normal directions is given by

$$\frac{\tau^{11}}{\tau^{22}} = \frac{\tau^{11}}{\tau^{33}} = \frac{-1.67}{-0.67} = 2.5$$

These same final relationships also apply to spherical one-dimensional geometry. In this case

$$\varepsilon^{22} = \varepsilon^{33} \neq 0$$

but the other equations are identical.

In one-dimensional cylindrical geometry

$$\varepsilon^{11} \neq 0$$
$$\varepsilon^{22} \neq 0$$
$$\varepsilon^{33} = \varepsilon^{12} = \varepsilon^{23} = \varepsilon^{13} = 0$$

This leads to the equation

$$\varepsilon^{11} + \varepsilon^{22} = -\Delta$$

But the dilatation, Δ, is usually quite small so that the following approximation is valid:

$$\varepsilon^{11} + \varepsilon^{22} = 0$$

or

$$d\varepsilon^{11} = -d\varepsilon^{22} \text{ and } d\varepsilon^{33} = 0$$

therefore

$$d\tau^{22} = -d\tau^{11} \text{ and } d\tau^{33} = 0$$

Placing these relations into the yield surface equation leads to

$$(d\tau^{11})^2 + (d\tau^{11})^2 - (d\tau^{11})^2 = Y^2/3$$
$$d\tau^{11} = -Y/\sqrt{3}$$
$$\tau^{11} = -Y/\sqrt{3} - P = -1.58P$$
$$\tau^{33} = 0 - P = -P$$
$$\tau^{22} = Y/\sqrt{3} - P = -0.42P$$

By definition, the "1" direction is the radial direction. The "2" direction is the hoop direction. And the "3" direction is an axial direction normal to the plane containing the cylindrical cross-section. The relations just developed then predict that the ratio of axial to radial stress is given by

$$\frac{\tau^{33}}{\tau^{11}} = \frac{-1.0}{-1.58} = 0.6$$

The relationships between stress components, which were developed above, will be very useful in understanding and analyzing calculational loading results.

The loading model developed in this study assumes a very large shock impedance mismatch between the concrete and the penetrator. The mismatch is required because the calculations used to develop the loading model assume no transmission of shock waves from the concrete into the penetrator. A steel penetrator would meet this criterion.

SECTION III
ELEMENT LOADING CALCULATIONS

The HULL (REF 2) and TOODY (REF 3) hydrocodes were used to investigate loading on simple one- and two-dimensional element shapes impacting 5,000 PSI unconfined compressive strength concrete. The simple shapes are seen in Figure 1. In the cylindrical and spherical cases the radii of curvature were varied from 5 to 20 cm. Velocities were varied from 50 to 500 m/sec. In the slab section calculations, angles between the surface normal and the velocity vector were varied from 0 to 60 degrees.

In all calculations the element surface velocity was held constant and the calculation was run until a steady stress level was attained.

Figure 2 shows typical results from TOODY calculations of slabs. The top figure presents stress in kilobars versus time in microseconds on a plane wall, or slab, being driven with a velocity of 300 m/sec applied at an angle of 30 degrees to the surface normal. Because of the hysteretic nature of the concrete stress versus strain relationship and the very low amount of viscosity used in the TOODY runs, the stress is initially very highly oscillatory and retains an approximately 10-percent oscillation after 20 microseconds. The true solution is shown as a smooth curve drawn through the center of the oscillations. The bottom figure presents the same information for a 300-m/sec velocity applied at an angle of 45 degrees to the surface normal. There is a slight peak in each smoothed curve followed by a steady value which eventually begins a slow decay from free surface relief. The steady value in the top curve is 14.5 kb and it is 10.8 kb in the bottom curve. With the velocity of 300 m/sec applied normally to the slab it was found that the steady stress was 17.2 kb. It is easily seen that the oblique impact values can be closely predicted by multiplying the normal impact value by the cosine of the velocity angle.

Results from one-dimensional plane and cylindrical calculations are seen in Figure 3. In the figure, steady stress in kb is plotted versus impact velocity in m/sec. The cylindrical calculations require separate curves to represent the radial and axial stress components. As discussed in Section II these components should be related by the equation

$$\frac{\tau \text{ axial}}{\tau \text{ radial}} = 0.6$$

It is clear in the figure that they are so related. It is also clear in the figure that the achieved stress level is very nearly

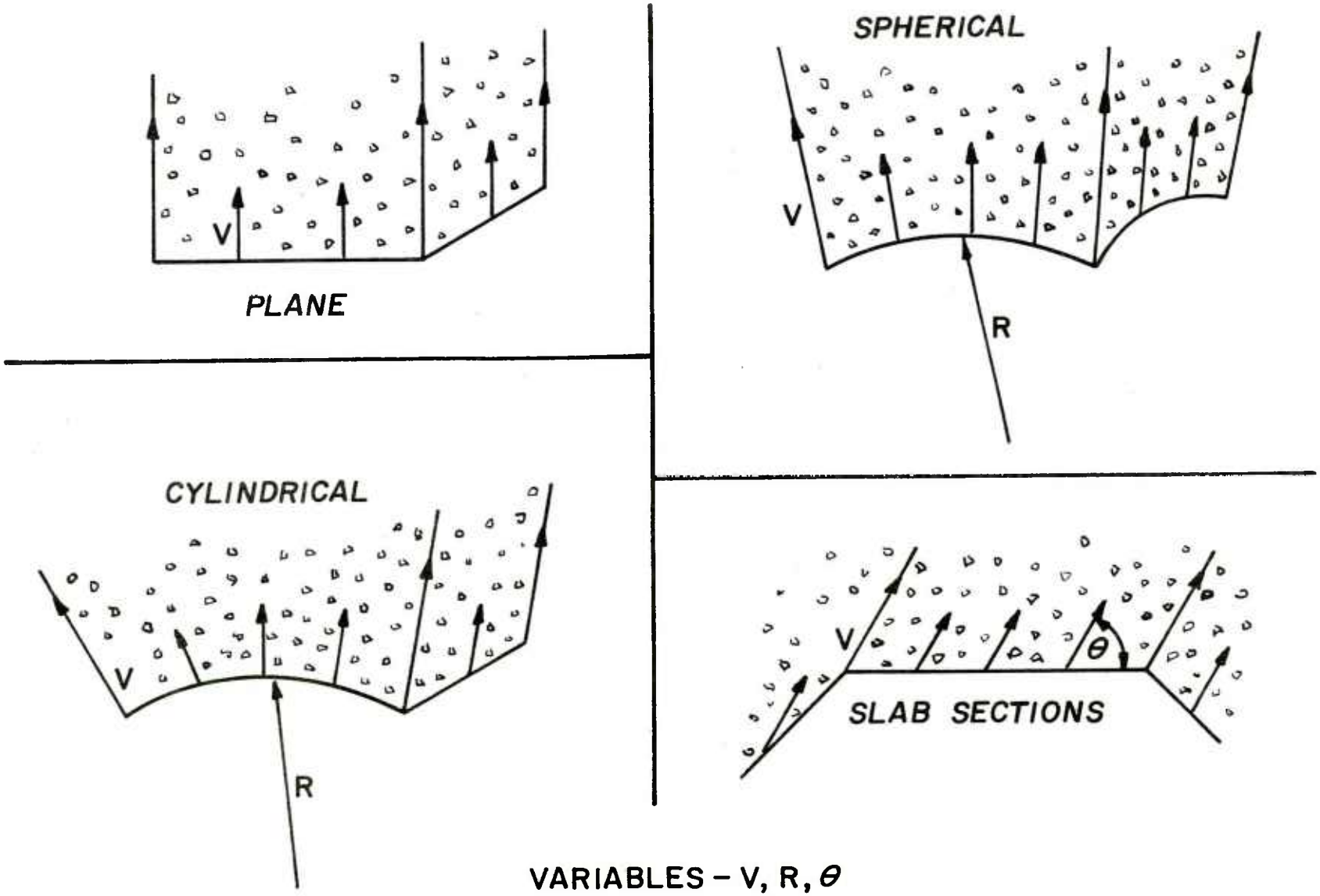

Figure 1. Geometric Shapes for Element Loading Calculations

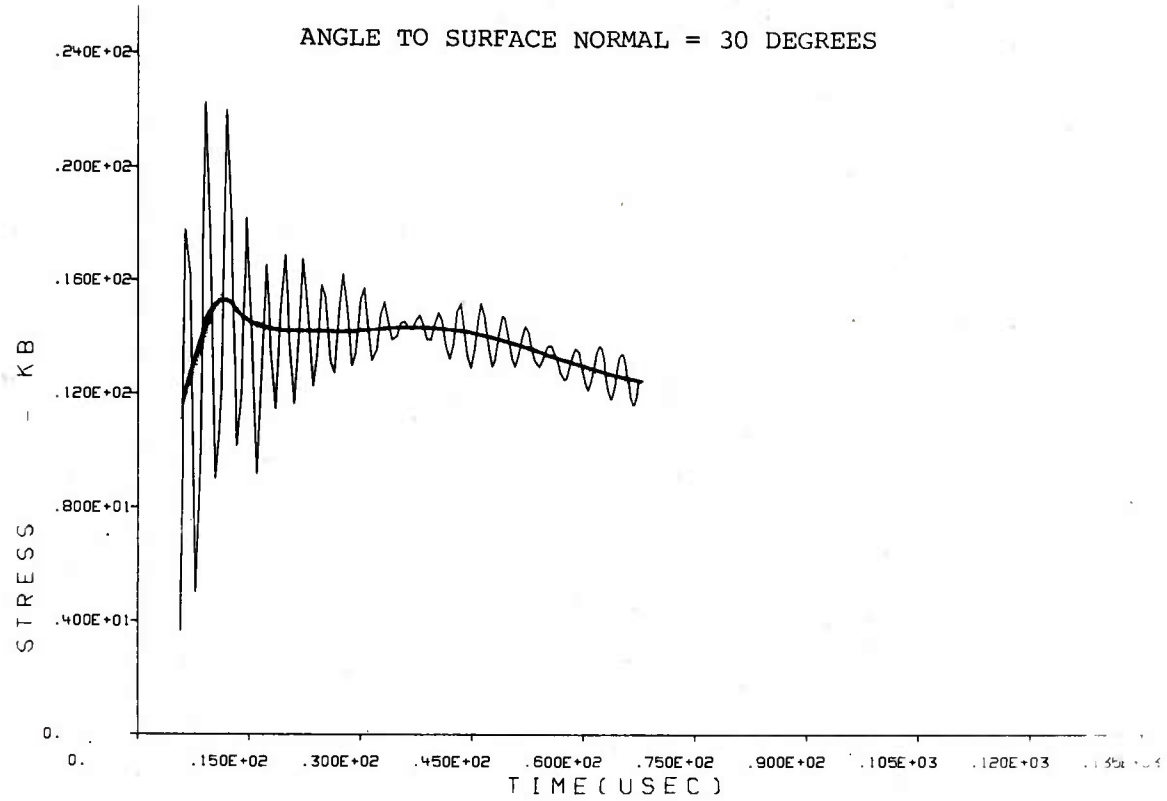

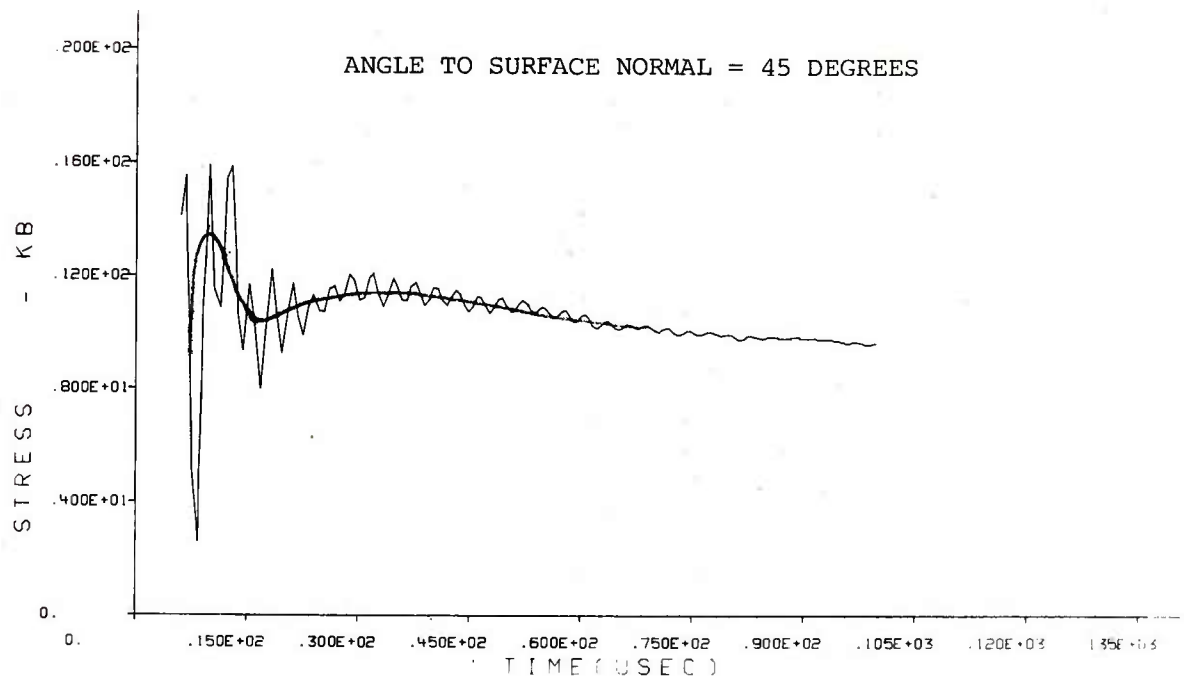

Figure 2. Stress Versus Time in TOODY Concrete Plane Wall Impacts at 300 m/s

a linear function of impact velocity. If τ is the stress loading in the dominant direction, then we can write

$$\tau = \rho c V$$

where ρ is the concrete's ambient density (2.2 g/cc), V is the impact velocity and c is an appropriate concrete sound speed. The plane and cylindrical one-dimensional cases and the two-dimensional slab cases can all be closely fit if c is set to 2.2×10^5 cm/sec. If V is also in cm/sec then τ will be in units of dynes/cm^2. Since 10^9 dynes/cm^2 is 1 kilobar, the conversion to kilobars is very simply made. The conversion to PSI can be made by noting that 69,000 dynes/cm^2 is 1 PSI.

Table I lists the results of several one-dimensional and slab geometry cases compared to the stress predicted from

$$\tau = 2.2 \times 2.2 \times 10^5 \times V \times \cos \Theta$$

where Θ is the angle between the velocity vector and the normal to the concrete surface. Most predictions are within 10 percent and all are within 23 percent. An even closer fit could be obtained were the fit made a function of the geometry (plane or cylindrical). However, it will be most useful to subsequent work to have a fit available which is not a function of geometry and a 23 percent error is considered to be well within the error expected when the loading is applied to various concrete mixtures and strengths. Fortunately, also, the radius of curvature makes little difference in cylindrical or spherical geometries. Thus the one fit can be used to describe the steady stress expected for all cases of interest to be encountered by penetrator surface elements in a terradynamics code.

To address peak stresses which will occur prior to the steady stress level and any dropoff from the steady stress level requires three-dimensional calculations. Of course, normal impacts of circular cross-section penetrators in three dimensions can be represented in two-dimensional axisymmetric coordinates. Several circular cross-section penetrators were examined in an attempt to understand initial and late-time stress loading. Figure 4 shows the two basic geometries examined--blunt and conically nosed penetrators.

The blunt-nosed penetrators were run in HULL at 100, 200, 300 and 500 m/sec. Figure 5 presents plots of stress levels on the penetrator noses as functions of time for the specified velocity levels. All penetrators were 1 cm in radius and were not allowed to slow down due to the applied stress. Stress values in the plot were determined by summing the force on all nose zones and dividing by the penetrator's cross-sectional area (π).

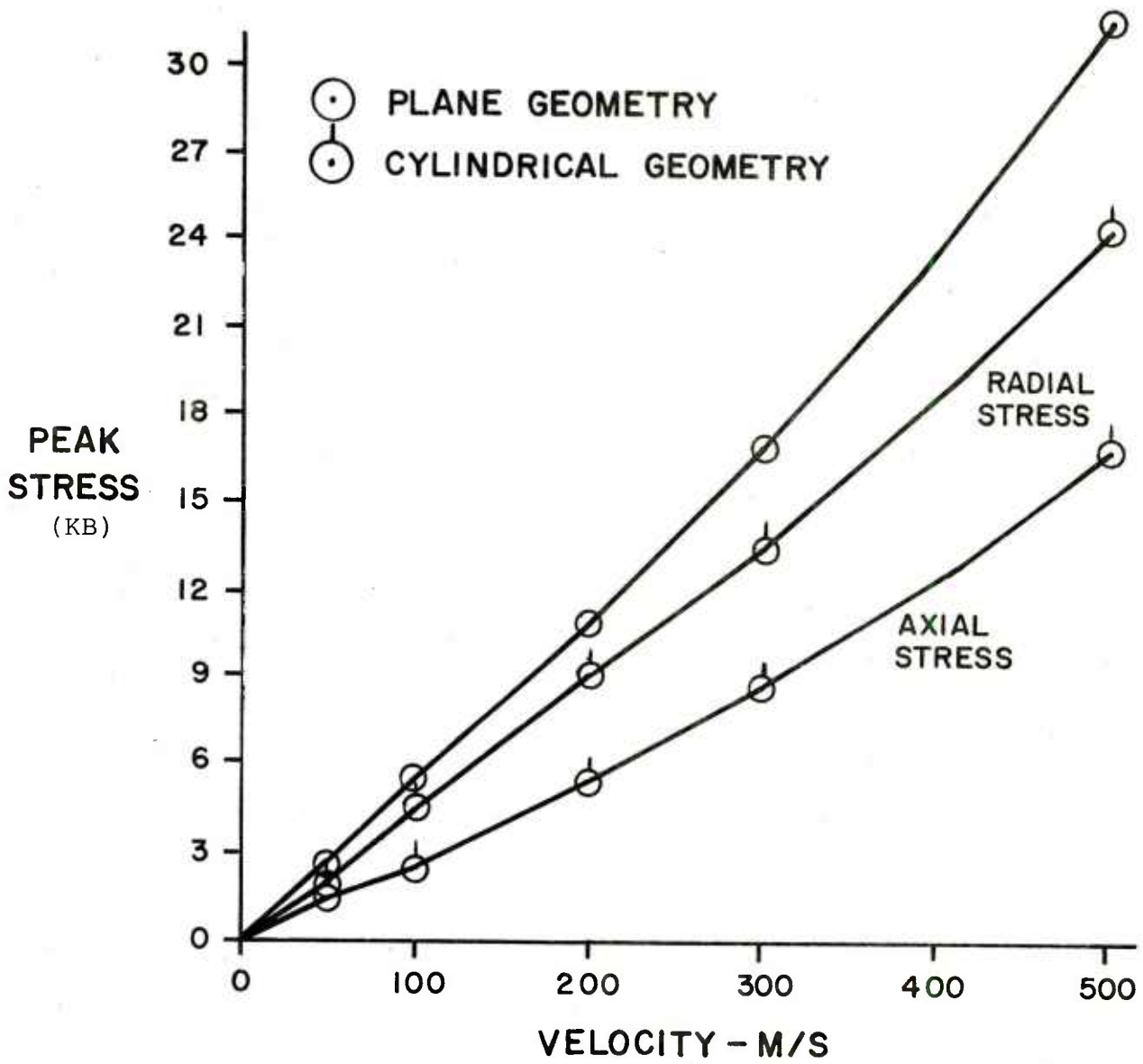

Figure 3. Steady Stress Values from One-Dimensional Calculations

TABLE I
TYPICAL ELEMENT LOADING CALCULATIONS

CALCULATIONAL GEOMETRY	VELOCITY-M/SEC	CALCULATED STRESS-KB	PREDICTED STRESS-KB	PERCENT ERROR
PLANE	50	2.7	2.4	-10.4
PLANE	100	5.2	4.8	- 6.9
PLANE	200	10.7	9.7	- 9.5
PLANE	300	17.2	14.5	-15.6
PLANE	500	31.5	24.2	-23
PLANE 30 degrees	300	14.5	12.6	-13.3
PLANE 45 degrees	300	10.8	10.3	- 4.9
CYLINDRICAL, R=10CM	50	2.3	2.4	5.2
CYLINDRICAL, R-10CM	100	4.8	4.8	0
CYLINDRICAL, R=10CM	200	9.3	9.7	4.1
CYLINDRICAL, R=10CM	300	13.7	14.5	6.0
CYLINDRICAL, R-10CM	500	25.5	24.2	-5.1
CYLINDRICAL, R=5CM	300	13.3	14.5	8.9
CYLINDRICAL, R-5CM	500	25.4	24.2	-4.7
SPHERICAL, R=10CM	300	12.9	14.5	-12.4

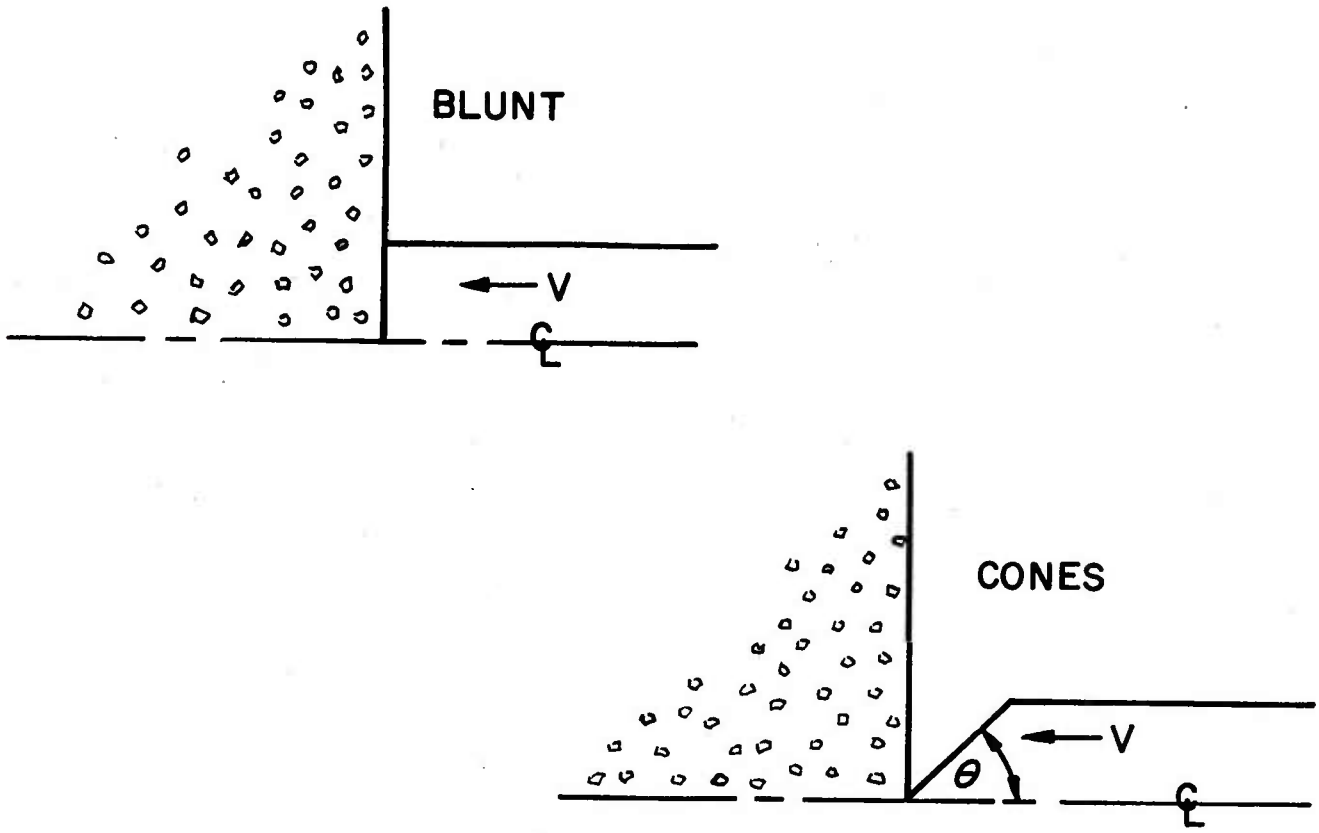

Figure 4. Circular Cross-Section Penetrator Geometries

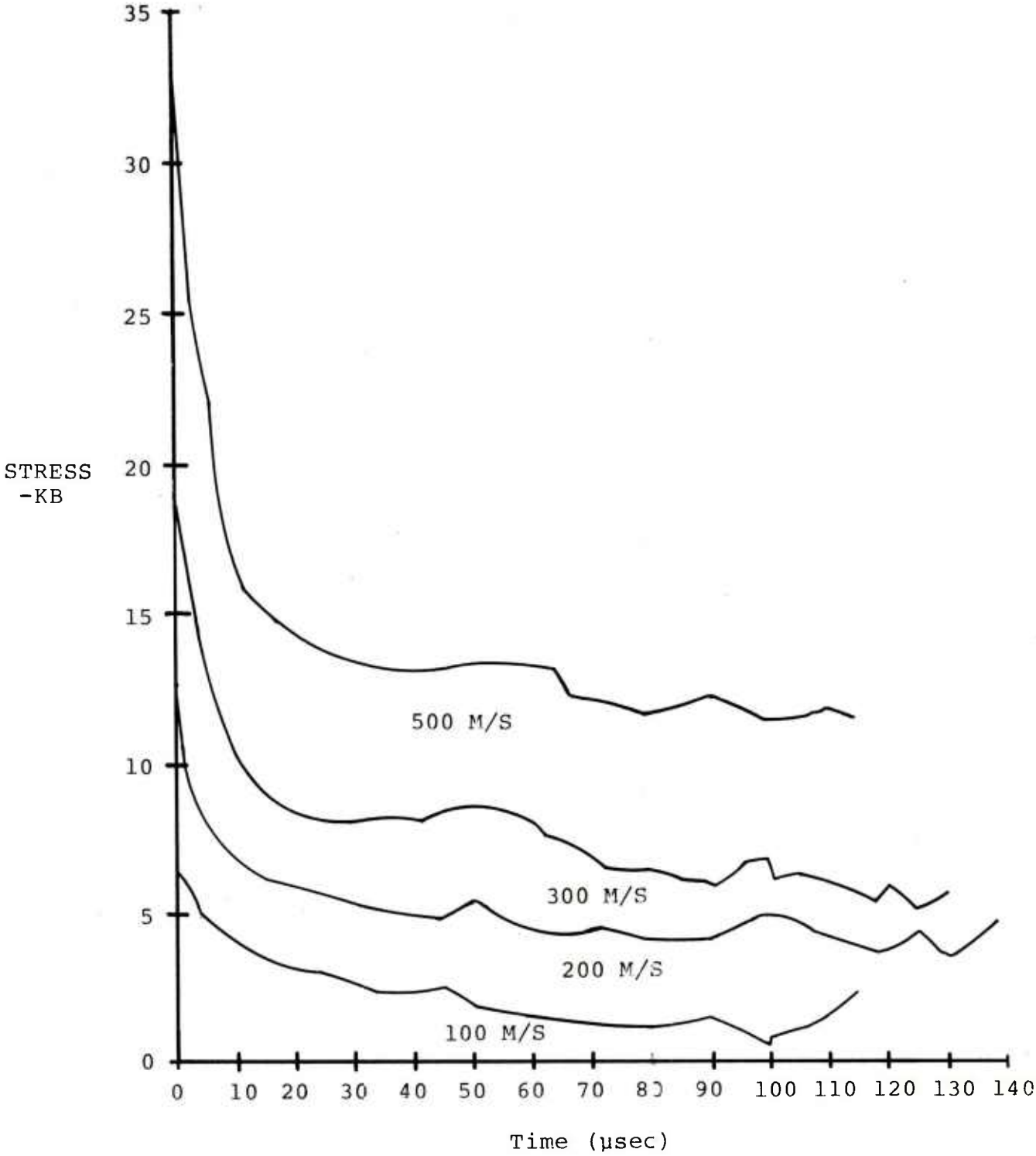

Figure 5. Blunt Projectile Stress Histories/ 5000 PSI Concrete

To understand this loading it must be examined in finer detail. Figure 6 shows the radial, axial and hoop stresses as well as the mean stress (-pressure) for time history station 1, for a blunt projectile impacting concrete at 300 m/sec. Time history station 1 is on the projectile's axis of symmetry. Only the axial stress component contributes to slowing down the penetrator. This axial component is initially very high and follows the cylindrical flow equations where the cylinder's radial direction is in the direction of motion of the penetrator. This flow rapidly changes to a cylindrical flow pattern in which the cylinder's radius is normal to the direction of motion of the penetrator. Thus the axial stress changes from the maximum stress component to 0.6 times the maximum stress component as the dominant direction of flow changes in the concrete. And the maximum stress itself changes from a peak value determined by setting c to 2.9×10^5 cm/sec.

With this background the axial stress seen in Figure 5 can now be understood. The peak values calculated from

$$\tau_{peak} = 2.2 \times 2.9 \times 10^5 \times V$$

decay to steady values which are approximately given by

$$\tau_{steady} = 0.6 \times 2.2 \times 2.2 \times 10^5 \times V$$

where the 0.6 factor takes into account the fact that the axial stress is not the dominant direction. At the time the steady stress level occurs, the concrete is predominantly being driven radially away from the penetrator. This steady stress value begins ultimately to decay as relief waves from the entrance free surface begin to overcome the axial loading.

The effect of a conical nose on peak and steady stress levels can be seen in Figure 7. In this figure axial stress is plotted versus time for three penetrator shapes impacting at 300 m/sec. The shapes are the blunt nose, a 45-degree half angle cone and a 60-degree half angle cone. Stress is seen to build up more slowly for the conical penetrators since the force on the penetrator is divided by the maximum cross-sectional area to obtain stress, even when the entire area is not in contact with the concrete. Table II provides a comparison of calculated peak and steady axial stress values for several blunt and conical-nosed penetrators. In this table the axial stress for cones is computed by considering the area actually in contact with the concrete. The equations previously discussed for peak and steady loading provide very accurate predictions for all of the cases studied when it is noted that the penetrator's velocity, V, must be multiplied by $\sin^2\theta$, where θ is the cone's half angle. This factor takes into account the fact that $V\sin\theta$ is the velocity applied to

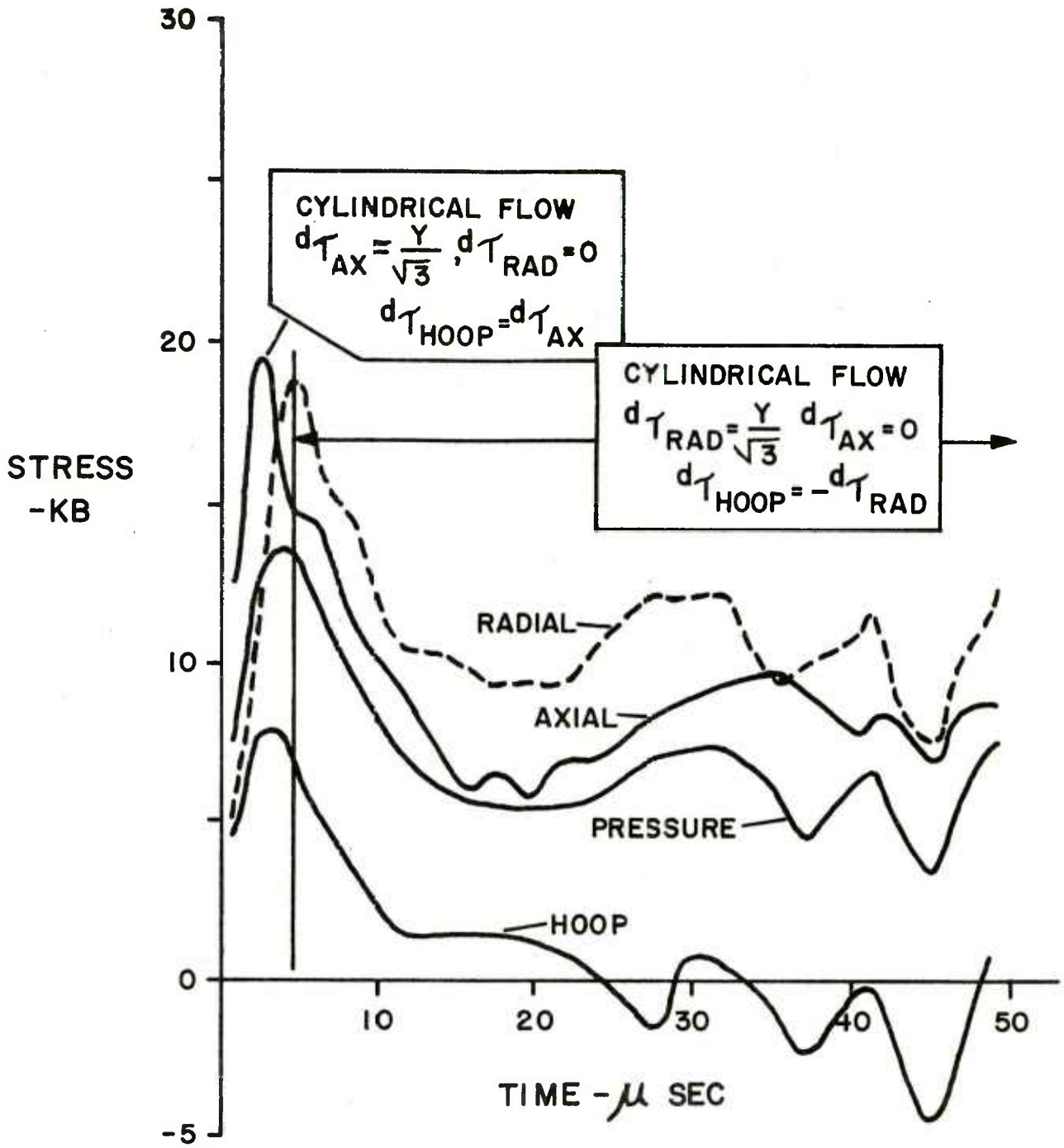

Figure 6. Station 1 Stresses for a Blunt Projectile at 300 m/sec

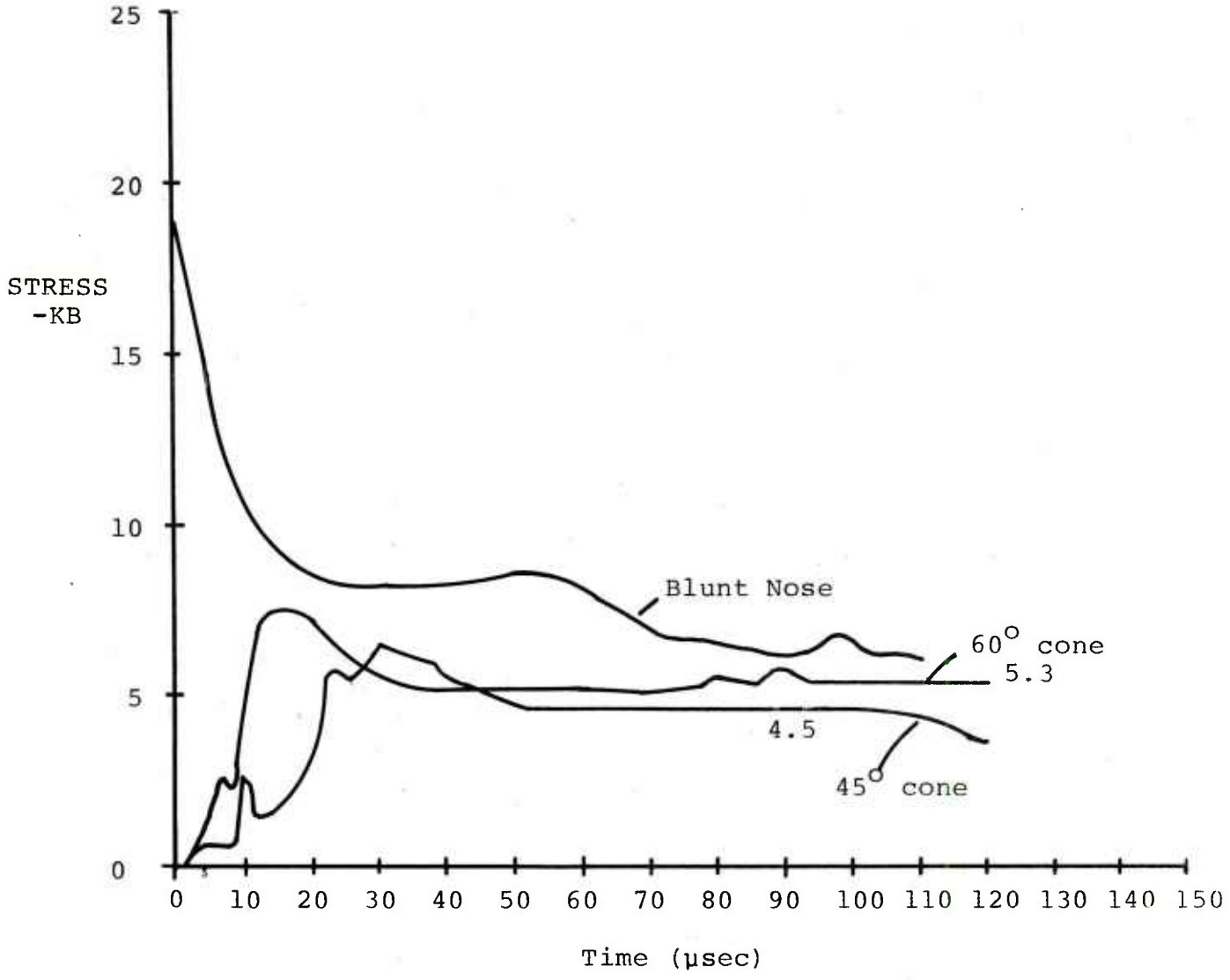

Figure 7. Axial Stress at 300 m/sec for Various Penetrator Noses

the concrete and $V\sin^2\theta$ is the component of that velocity in the axial direction.

The time required to decay from peak to steady stress levels can be expected to be a function of the penetrator's diameter. It does not appear to be a very strong function of the penetrator's velocity. Figure 8 presents axial stress versus time for blunt penetrators with radii of 1 and 2 cm. The time required to decay to steady values appears to be a linear function of the size of the penetrator. Based on these two calculations and comparisons with the other 1-cm radius penetrator loads, it appears that the time to decay from peak to steady stress levels can be approximately expressed as

$$T = 14 \times 10^{-6} \times D(\text{cm}) \text{ sec.}$$

Where D is the penetrator's diameter, it also appears that a straight line adequately describes this drop in stress level with time.

Eventually, rarefactions from the entrance free surface reduce the stress loading on the penetrator. All compressive waves generated in the concrete eventually generate relief waves at the free surface. Geometrical divergence of the compressive waves and subsequent divergence of the relief waves generated by them insure that the rarefactions cannot individually reduce loading by any significant amount. However, after a relatively long period of time these relief waves are capable of almost totally reducing all compressive loading on the penetrator.

It is reasonable to suppose that the time required for entrance surface relief waves to significantly affect loading will be a function of velocity. The penetrator will be further from the surface, at some given time, at a higher velocity. And, in fact, the calculations indicate that this is true. For blunt projectiles, at 100 m/sec velocity, loading is significantly reduced by 45 μsec. This time rises to 50 μsec for a velocity of 200 m/sec, 60 μsec at a velocity of 300 m/sec and 70 μsec at 500 m/sec. These times can be expressed in terms of a number of wave transits from the free surface to the penetrator's centerline. For example, for the 100 m/sec penetrator the initial distance to the free surface is 0.5D where D is the diameter of the penetrator. At 45 microseconds the distance to the free surface is 0.5D plus the depth of penetration of 100 m/sec x 100 cm/m x 45 μsec = 0.45 cm. The average distance, therefore, from the penetrator centerline to the free surface is 0.5 x (1 cm + 1.45 cm) or 1.2 cm. Assuming a sound speed in the concrete of 2.2×10^5 cm/sec, the average distance of 1.2 cm represents 8.2 transits. Similarly, the 200 m/sec penetrator begins to lose steady stress at 7.3 transits, the 300 m/sec penetrator loses stress at 6.9 transits and

TABLE II
PEAK AND STEADY STRESSES ON VARIOUS PENETRATORS

PENETRATOR	VELOCITY M/SEC	CALCULATED PEAK STRESS (KB)	PREDICTED PEAK STRESS (KB)	PERCENT ERROR	CALCULATED STEADY STRESS (KB)	PREDICTED STEADY STRESS (KB)	PERCENT ERROR
BLUNT	100	6.5	6.4	-1.5	3.0	2.9	-3.4
BLUNT	200	12.5	12.8	2.4	5.5	5.8	5.5
BLUNT	300	19	19.1	0.5	8.5	8.7	2.3
BLUNT	500	33	31.9	-3.3	13.5	14.5	7.4
45 Degree Cone	200	6.1	6.4	4.9	3.0	2.9	-3.4
45 Degree Cone	300	9.7	9.6	1.0	4.5	4.4	-2.2
60 Degree Cone	300	16	14.4	-10.0	5.3	6.5	22.6

Peak Stress predicted from

$$\tau(\text{dynes/cm}^2) = 2.2 \times 2.9 \times 10^5 \times V\ (\text{cm/sec}) \times \sin^2\theta$$

Steady Stress predicted from

$$\tau(\text{dynes/cm}^2) = 0.6 \times 2.2 \times 2.2 \times 10^5 \times V\ (\text{cm/sec}) \times \sin^2\theta$$

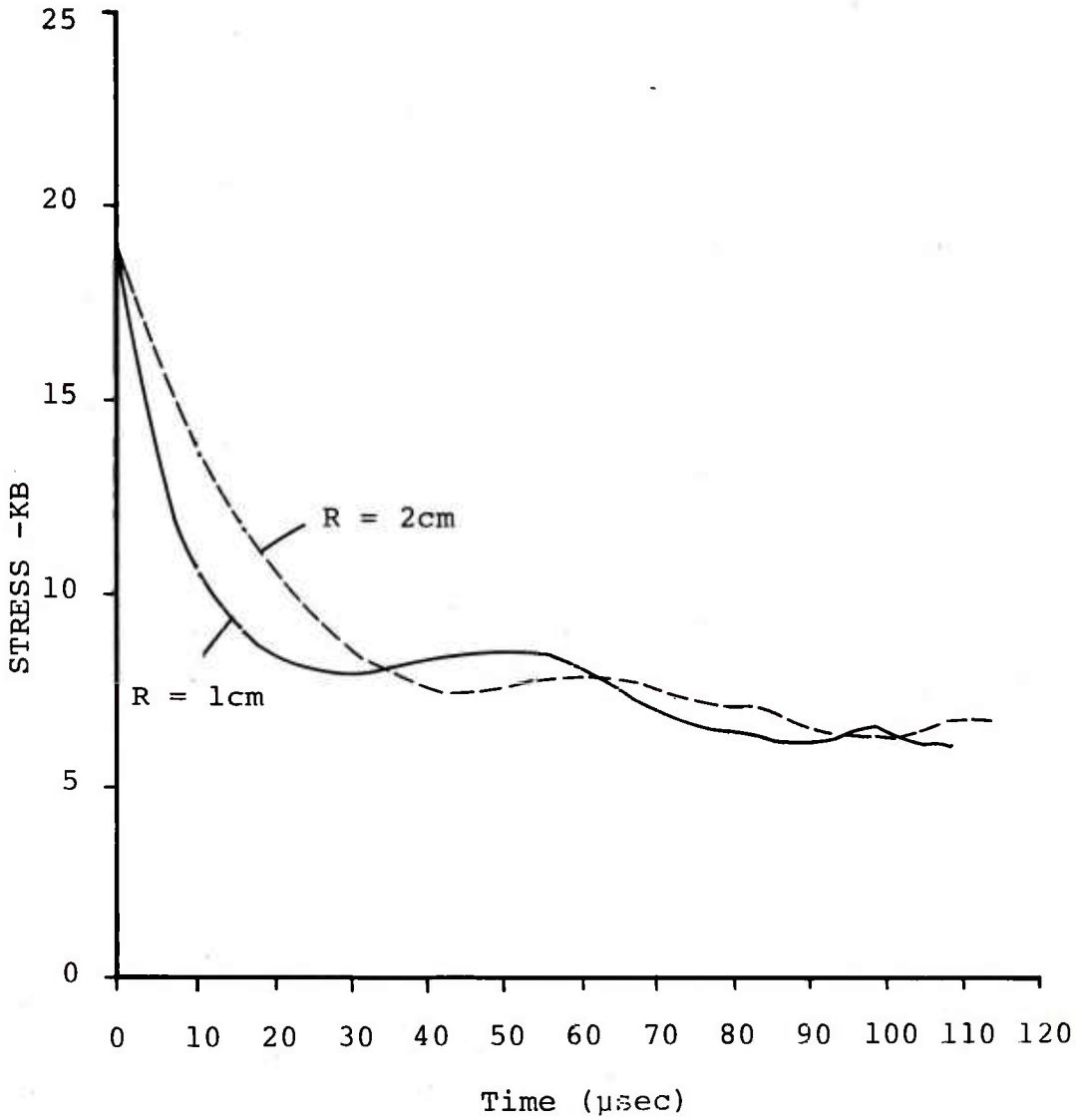

Figure 8. Blunt Projectiles Impacting Concrete at 300 m/sec

the 500 m/sec significantly loses stress at 5.6 transits. The number of transits is a relatively linear function of velocity and is expressed by

$$A = 8.2 - (V\text{-}1 \times 10^{4}) \times 65 \times 10^{-6}$$

where A is the number of transits and V is the velocity in cm/sec. The time, in seconds, at which the steady stress begins to significantly decay can then be expressed as

$$T = A \times D/(c - 0.5 \times A \times V)$$

where D is the diameter of the projectile in cm, V is its velocity in cm/sec and c is the sound speed 2.2×10^{5} cm/sec.

For all of the blunt projectiles run in this study the stress loss per unit time is a constant 0.031 kb/μsec. Computer time was not available to run any of the projectiles to the point at which the stress no longer decreased. However, for the purpose of model building it will be assumed that loss will continue until the stress level is reduced to that which would occur due to simply pushing completely fractured concrete, i.e., $\frac{1}{2}\rho V^{2}$.

SECTION IV
THE ELEMENT LOADING MODEL

The penetrator element loading model resulting from this analysis is seen in Figure 9. The model is presented in terms of applied stress in dynes/cm^2 versus time in seconds. Stress levels are computed from V_N, the velocity component normal to the element's surface. Stress levels are connected linearly between the initial time of impact and times T_1 (the time of peak stress clearing), T_2 (the time at which relief waves from the entrance free surface significantly affect loading) and T_3 (the time at which applied stress results from simply pushing failed concrete).

The majority of a penetrator's loading will result from the relatively long steady stress level of $0.6 \times 2.2 \times 2.2 \times 10^5 \times V_N$. Using this predominant stress level, drag coefficients for a normally impacting projectile can be computed. If A is the projectile's cross-sectional area, V its velocity, m its mass and C_D its drag coefficient, then

$$m \times \dot{V} = \tau \times A = -\rho \times C_D \times A \times V^2/2$$

or

$$C_D = 2\tau/\rho V^2$$

substituting the steady value for τ yields

$$C_D = 2 \times 0.6 \times 2.2 \times 2.2 \times 10^5 \times V/(2.2 \times V^2)$$
$$C_D = 2.64 \times 10^5/V$$

Thus C_D is an inverse function of velocity. This means that as the projectile slows its drag coefficient increases. Figure 9 is a plot of this drag coefficient for blunt projectiles versus projectile velocity. It is seen that C_D significantly increases as velocity decreases below 200 m/sec.

This is an interesting function for C_D since it means that projectiles will actually eventually stop as opposed to the endless trajectory resulting from a constant C_D model.

The drag equation for blunt projectiles becomes

$$\dot{V} = -\rho \times C_D \times A \times V^2/(2 \times m)$$
$$= 2.2 \times 1.2 \times 2.2 \times 10^5 \times A \times V/(2 \times m)$$
$$= 2.9 \times 10^5 \times A \times V/m$$

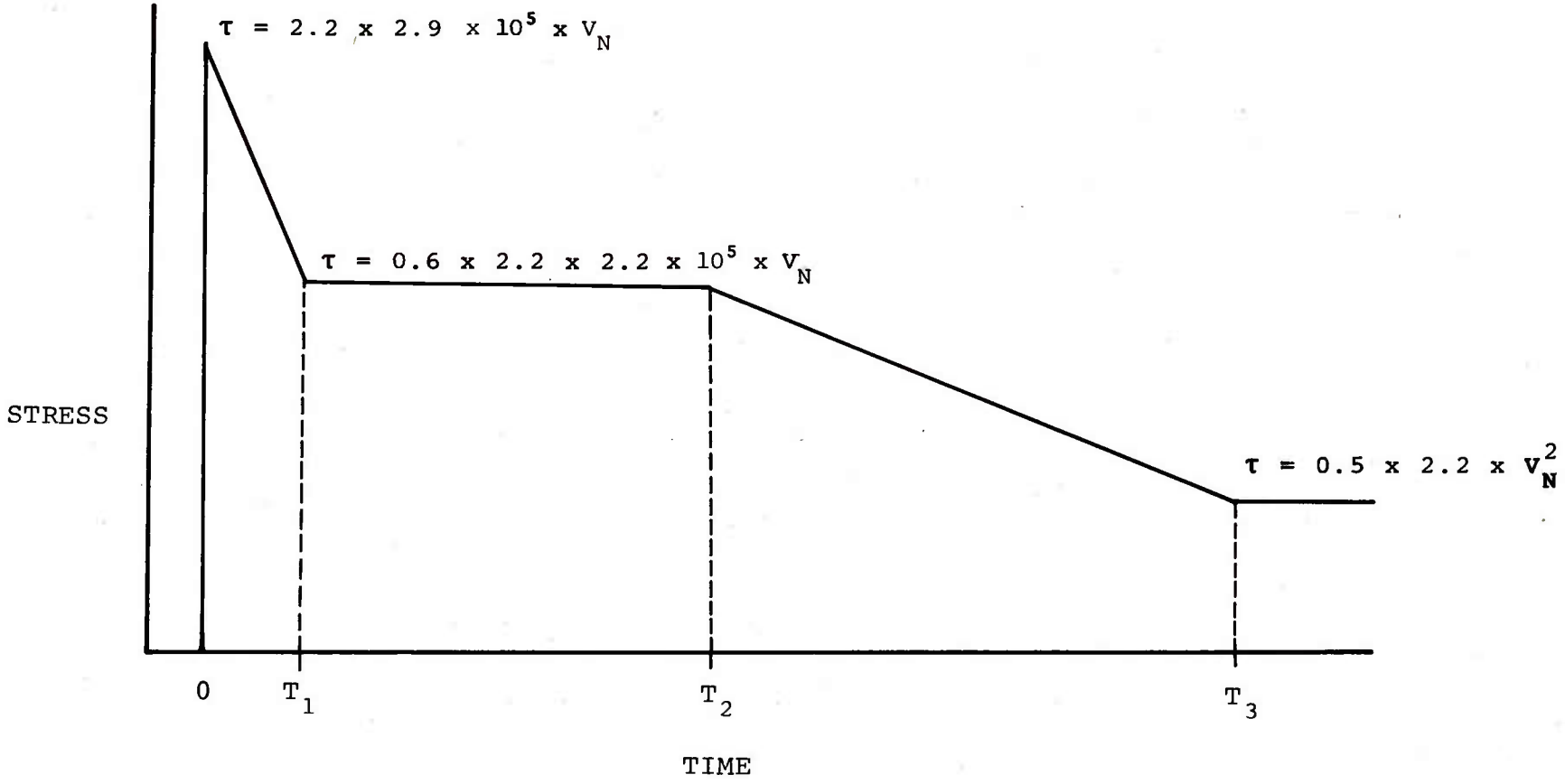

$T_1 = 14 \times 10^{-6} \times D(cm)$, D = diameter of element

$T_2 = A \times D/(C-0.5 \times A \times V_N)$, $A = 8.2 - (V_N - 1 \times 10^4)\ 65 \times 10^{-6}$

$T_3 = \rho \times V_N \times (0.6 \times C - 0.5 \times V_N)\ 3.33 \times 10^{-8}$

$\rho = 2.2$ gm/cc $C = 2.2 \times 10^5$ cm/sec

Figure 9. The Element Loading Model

which has the solutions

$$V = V_o \, e^{(-2.9 \times 10^5 \times A/m)t}$$

and

$$s = (V-V_o) \; / \; (-2.9 \times 10^5 \times A/m)$$

Where s is the depth of penetration, V_o is the initial velocity and V is the velocity at time t. These equations predict a finite depth of penetration since substitution of V = 0 in the equation for s yields

$$S_{final} = V_o \; / \; (2.9 \times 10^5 \times A/m)$$

Similar equations can be developed for conically nosed penetrators by simply substituting $V\sin^2\theta$ for V, where θ is the cone's half angle.

These equations were used to predict penetration depth at various times for blunt projectiles run in HULL with forces being allowed to actually slow the projectiles. Two cases were run. In each case the projectile weighed 500 gm and its cross-section area was 3.14 cm^2. In the first case impact occurred at 500 m/sec and HULL predicted a velocity of 393 m/sec at a time of 150 μsec and a depth in the semi-infinite concrete of 6.57 cm. The simplified equations for velocity and depth predicted a velocity of 380 m/sec and a depth of 6.25 cm at 150 μsec. This is less than a 5-percent error in each quantity. In the second case, the projectile impacted at 200 m/sec and the HULL run predicted a velocity of 150 m/sec and a depth of 3.31 cm at a time of 193 μsec. The simple model predicted a velocity of 141 m/sec and a depth of 3.25 cm at a time of 193 μsec. These predictions are again within a 5-percent error.

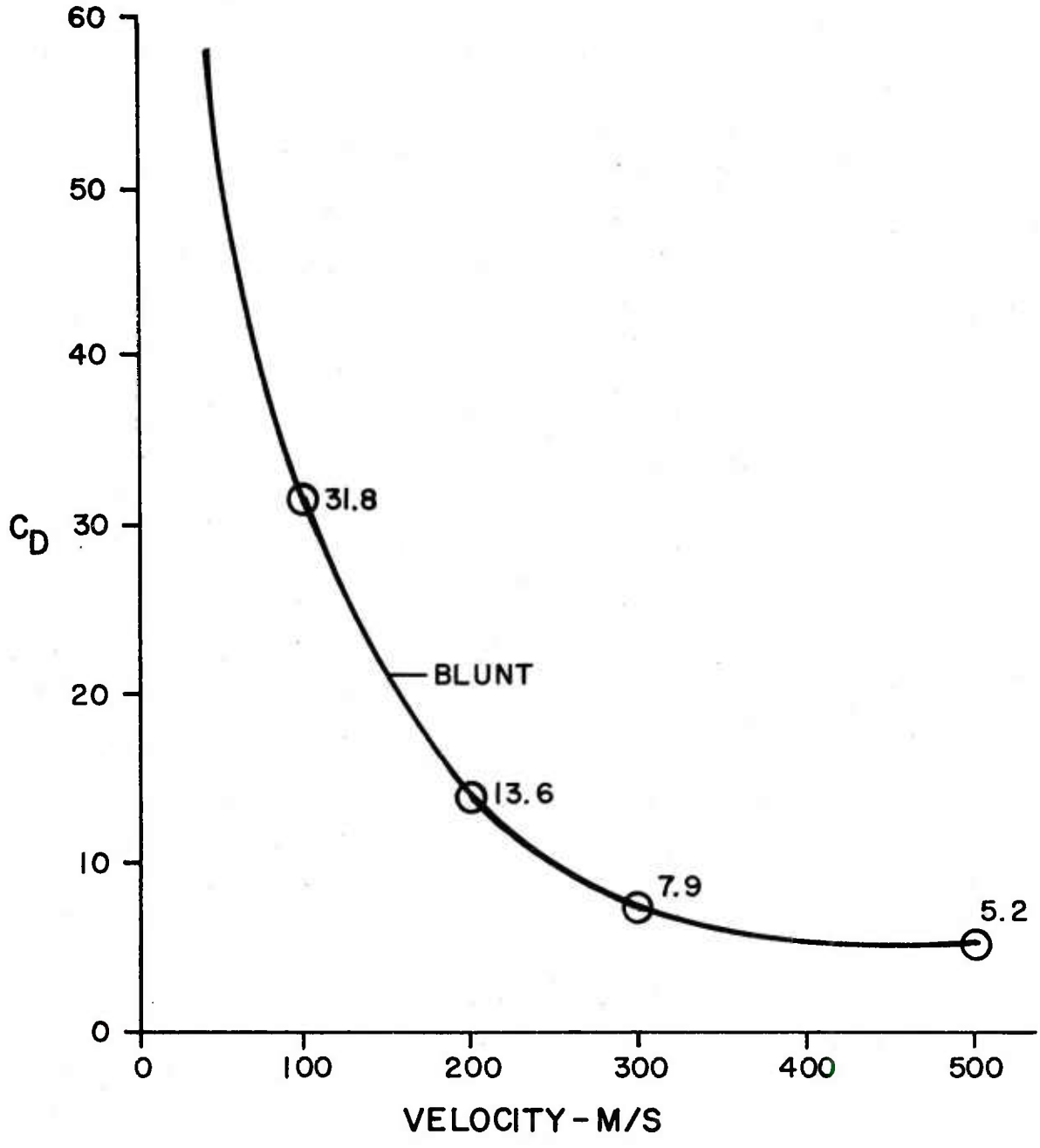

Figure 10. Drag Coefficient for Blunt Projectiles

SECTION V
RECOMMENDED FUTURE WORK

Several critical technical issues should be resolved prior to application of the suggested loading model in simplified terradynamics codes. These issues are discussed below.

The existence of the 0.6 stress multiplication factor should be verified in three-dimensional oblique flow fields. It is believed that the factor will be valid in these flows since the projectile element is pushing concrete basically radially away from itself.

The time at which the steady stress begins to decrease due to entrance surface relief waves should be investigated in three-dimensional oblique impacts. The simplified equation used in the model described in this report assumes a single distance from the element to the surface. In an oblique impact there are a multitude of such distances associated with every element.

Effects of interfering flow fields between elements must also be investigated in three-dimensional impacts. The loading model assumes that flow past neighboring elements has no influence on the element in question.

The model assumes a semi-infinite concrete thickness. There are, of course, no such concrete structures in this world. Loading in penetration of a finite thickness concrete slab will differ from semi-infinite loading as soon as the initial compressive wave generated at impact reflects as a tensile wave from the exit free surface and reaches the projectile nose.

Further work on this model should concentrate on the loading perturbations seen because of the concrete slab's finite thickness. When this stress decrement is accounted for, the three-dimensional effects mentioned above should be addressed.

REFERENCES

1. Osborn, J. J. and Matuska, D. A., "Dynamic Response of a Kinetic Energy Penetrator - Hydrocode Analysis of a Kinetic Energy Penetration Into Concrete", AFATL-TR-78-24, Vol II, Air Force Armament Laboratory, March 1978.

2. Matuska, D. A. and Durrett, R. E., "The HULL Code, A Finite Difference Solution to the Equations of Continuum Mechanics", AFATL-TR-78-125, Air Force Armament Laboratory, November 1978.

3. Swegle, J. W., "TOODY-IV, A Computer Program for Two-Dimensional Wave Propagation", SAND-78-0552, Sandia Laboratories, September 1978.

DISTRIBUTION LIST

No. of Copies	Organization
12	Commander Defense Technical Info Center ATTN: DDC-DDA Cameron Station Alexandria, VA 22314
1	Director Defense Advanced Research Projects Agency ATTN: Tech Info 1400 Wilson Boulevard Arlington, VA 22209
1	Director Defense Nuclear Agency Washington, DC 20305
1	Deputy Assistant Secretary of the Army (R&D) Department of the Army Washington, DC 20310
2	Commander US Army BMD Advanced Technology Center ATTN: BMDATC-M, Mr. P. Boyd Mr. S. Brockway PO Box 1500 Huntsville, AL 35807
1	HQDA (DAMA-ARP) WASH DC 20310
1	HQDA (DAMA-MS) WASH DC 20310
2	Commander US Army Engineer Waterways Experiment Station ATTN: Dr. P. Hadala Dr. B. Rohani PO Box 631 Vicksburg, MS 39180
1	Commander US Army Materiel Development and Readiness Command ATTN: DRCDMD-ST 5001 Eisenhower Avenue Alexandria, VA 22333
10	Commander US Army armament Research and Development Command ATTN: DRDAR-TD, Dr. R. Weigle DRDAR-LC, Dr. J. Frasier DRDAR-SC, Dr. D. Gyorog DRDAR-LCF, G. Demitrack DRDAR-LCA, G. Randers-Pehrson DRDAR-SCS-M, R. Kwatnoski DRDAR-LCU, E. Barrieres DRDAR-SCM, Dr. E. Bloore DRDAR-TSS (2 cys) Dover, NJ 07801
2	Director US Army ARRADCOM Benet Weapons Laboratory ATTN: DRDAR-LCB-TL Dr. Joseph E. Flaherty Watervliet, NY 12189
1	Commander US Army Armament Materiel Readiness Command ATTN: DRSAR-LEP-L, Tech Lib Rock Island, IL 61299
1	Commander US Army Aviation Research and Development Command ATTN: DRDAV-E 4300 Goodfellow Blvd. St. Louis, MO 63120

DISTRIBUTION LIST

No. of Copies	Organization
1	Director US Army Air Mobility Research and Development Laboratory Ames Research Center Moffett Field, CA 94035
1	Commander US Army Communications Research and Development Command ATTN: DRDCO-PPA-SA Fort Monmouth, NJ 07703
1	Commander US Army Electronics Research and Development Command Technical Support Activity ATTN: DELSD-L Fort Monmouth, NJ 07703
1	Commander US Army Missile Command ATTN: DRSMI-R Redstone Arsenal, AL 35809
1	Commander US Army Missile Command ATTN: DRSMI-RBL Redstone Arsenal, AL 35809
1	Commander US Army Missile Command ATTN: DRSMI-YDL Redstone Arsenal, AL 35809
2	Commander US Army Tank Automotive Research & Development Cmd ATTN: DRDTA-UL V. H. Pagano Warren, MI 48090
1	Commander TARADCOM Tank Automotive Systems Laboratory ATTN: T. Dean Warren, MI 48090
6	Director US Army Materials and Mechanics Research Center ATTN: DRXMR-T, Mr. J. Bluhm Mr. J. Mescall Dr. M. Lenoe R. Shea F. Quigley DRXMR-ATL Watertown, MA 02172
2	Commander US Army Research Office ATTN: Dr. E. Saibel Dr. G. Mayer PO Box 12211 Research Triangle Park NC 27709
1	Director US Army TRADOC Systems Analysis Activity ATTN: ATAA-SL (Tech Lib) White Sands Missile Range NM 88002
1	Office of Naval Research Department of the Navy ATTN: Code ONR 439, N. Perrone 800 North Quincy Street Arlington, VA 22217

DISTRIBUTION LIST

No. of Copies	Organization
3	Commander Naval Air Systems Command ATTN: AIR-604 Washington, DC 20360
3	Commander Naval Ordnance Systems Command Washington, DC 20360
2	Commander Naval Air Development Center, Johnsville Warminster, PA 18974
1	Commander Naval Missile Center Point Mugu, CA 93041
2	Commander Naval Ship Engineering Center ATTN: J. Schell Tech Lib Washington, DC 20362
1	Commander and Director David W. Taylor Naval Ship Research and Development Center Bethesda, MD 20084
2	Commander Naval Surface Weapons Center ATTN: Dr. W. G. Soper Mr. N. Rupert Dahlgren, VA 22448
4	Commander Naval Surface Weapons Center ATTN: Dr. S. Fishman (2 cys) Code U-11, J. R. Renzi R. S. Gross Silver Spring, MD 20910
6	Commander Naval Surface Weapons Center ATTN: Code R-13, F.J. Zerilli K. Kim E. T. Toton M. J. Frankel Code K-22, F. Stecher J. M. Etheridge Silver Spring, MD 20910
3	Commander Naval Weapons Center ATTN: Code 31804, Mr. M. Smith Code 326, Mr. P. Cordle Code 3261, Mr. T. Zulkoski China Lake, CA 93555
6	Commander Naval Weapons Center ATTN: Code 3181, John Morrow Code 3261, Mr. C. Johnson Code 3171, Mr. B. Galloway Code 3831, Mr. M. Backman Mr. R. E. VanDevender,Jr. Dr. O.E.R. Heimdahl China Lake, CA 93555
2	Director Naval Research Laboratory ATTN: Dr. C. Sanday Dr. H. Pusey Washington, DC 20375
2	Superintendent Naval Postgraduate School ATTN: Dir of Lib Dr. R. Ball Monterey, CA 93940

DISTRIBUTION LIST

No. of Copies	Organization
1	Long Beach Naval Shipyard ATTN: R. Kessler T. Eto R. Fernandez Long Beach, CA 90822
1	HQ USAF/SAMI Washington, DC 20330
1	AFIS/INOT Washington, DC 20330
10	ADTC/DLJW (MAJ G. Spitale) Eglin AFB, FL 32542
20	ADTC/DLYV (Mr. J. Collins) Eglin AFB, FL 32542
1	AFATL/DLYV Eglin AFB, FL 32542
1	AFATL/DLODL Eglin AFB, FL 32542
1	AFATL/CC Eglin AFB, FL 32542
1	AFATL/DLODR Eglin AFB, FL 32542
1	HQ PACAF/DOOQ Hickam AFB, HI 96853
1	HQ PACAF/OA Hickam AFB, HI 96853
1	OOALC/MMWMC Hill AFB, UT 84406
1	HQ TAC/DRA Langley AFB, VA 23665
1	TAC/INAT Langley AFB, VA 23665
1	AUL-LSE 71-249 Maxwell AFB, AL 36112
1	AFWAL/MLLN (Mr. T. Nicholas) Wright-Patterson AFB, OH 45433
1	ASD/ENESS (S. Johns) Wright-Patterson AFB, OH 45433
1	ASD/ENFEA Wright-Patterson AFB, OH 45433
1	ASD/XRP Wright-Patterson AFB, OH 45433
1	HQ USAFE/DOQ APO New York 09012
1	COMIPAC/I-32 Box 38 Camp H. I. Smith, HI 96861
10	Battelle Northwest Laboratories ATTN: G. D. Marr P. O. Box 999 Richland, WA 99352
1	Director Lawrence Livermore Laboratory ATTN: Ms. C. Westmoreland P. O. Box 808 Livermore, CA 94550

DISTRIBUTION LIST

No. of Copies	Organization
2	Lawrence Livermore Laboratory PO Box 808 ATTN: Dr. R. Werne Dr. J.O. Hallquist Livermore, CA 94550
6	Los Alamos Scientific Laboratory PO Box 1663 ATTN: Dr. R. Karpp Dr. J. Dienes Dr. J. Taylor Dr. E. Fugelso Dr. D. E. Upham Dr. R. Keyser Los Alamos, NM 87545
5	Sandia Laboratories ATTN: Dr. R. Woodfin Dr. M. Sears Dr. W. Herrmann Dr. L. Bertholf Dr. A. Chabai Albuquerque, NM 87115
1	Headquarters National Aeronautics and Space Administration Washington, DC 20546
1	Jet Propulsion Laboratory 4800 Oak Grove Drive ATTN: Dr. Ralph Chen Pasadena, CA 91102
1	Director National Aeronautics and Space Administration Langley Research Center Langley Station Hampton, VA 23365
1	US Geological Survey 2255 N. Gemini Drive ATTN: Dr. D. Roddy Flagstaff, AZ 86001
1	Aerojet Ordnance Company 9236 East Hall Road Downey, CA 90241
1	Aeronautical Research Associates of Princeton, Inc. 50 Washington Road Princeton, NJ 08540
1	Aerospace Corporation 2350 E. El Segundo Blvd. ATTN: Mr. L. Rubin El Segundo, CA 90009
1	AVCO Systems Division 201 Lowell Street ATTN: Dr. Reinecke Wilmington, MA 01803
4	Battelle Columbus Laboratories 505 King Avenue ATTN: Dr. M. F. Kanninen Dr. G. T. Hahn Dr. L. E. Hulbert Dr. S. Sampath Columbus, OH 43201
3	Boeing Aerospace Company ATTN: Mr. R. G. Blaisdell (M.S. 40-25) Dr. N. A. Armstrong, C. J. Artura (M.S. 8C-23) Seattle, WA 98124
2	Brunswick Corporation 4300 Industrial Avenue ATTN: P. S. Chang R. Grover Lincoln, NE 68504
1	Computer Code Consultants, Inc. 1680 Camino Redondo ATTN: Dr. Wally Johnson Los Alamos, NM 87544

DISTRIBUTION LIST

No. of Copies	Organization
1	Dresser Center PO Box 1407 ATTN: Dr. M.S. Chawla Houston, TX 77001
1	Effects Technology, Inc. 5383 Hollister Avenue Santa Barbara, CA 93111
2	Firestone Defense Research and Products 1200 Firestone Parkway ATTN: R. L. Woodall L. E. Vescelius Akron, OH 44317
1	FMC Corporation Ordnance Engineering Division San Jose, CA 95114
1	Ford Aerospace and Communications Corporation Ford Road, PO Box A ATTN: L. K. Goodwin Newport Beach, CA 92660
1	General Atomic Company PO Box 81608 ATTN: R. M. Sullivan F. H. Ho S. Kwei San Diego, CA 92138
1	General Dynamics PO Box 2507 ATTN: J. H. Cuadros Pomona, CA 91745
1	General Electric Company Armament Systems Department Burlington, VT 05401
1	President General Research Corporation ATTN: Lib McLean, VA 22101
1	Goodyear Aerospace Corporation 1210 Massilon Road Akron, OH 44315
1	H. P. White Laboratory 3114 Scarboro Road Street, MD 21154
4	Honeywell, Inc. Government and Aerospace Products Division ATTN: Mr. J. Blackburn Dr. G. Johnson Mr. R. Simpson Mr. K. H. Doeringsfeld 600 Second Street, NE Hopkins, MN 55343
1	Hughes Aircraft Corporation ATTN: Mr. W. Keppel MS M-5, Bldg. 808 Tucson, AZ 85706
1	International Applied Physics, Inc. ATTN: Mr. H. F. Swift 7546 McEwen Road Centerville, OH 45459
2	Kaman Sciences Corporation 1500 Garden of the Gods Road ATTN: Dr. P. Snow Dr. D. Williams Colorado Springs, CO 80933
1	Lockheed Palo Alto Research Laboratory 3251 Hanover Street ATTN: Org 5230, Bldg. 201 Mr. R. Robertson Palo Alto, CA 94394
1	Materials Research Laboratory, Inc. 1 Science Road Glenwood, IL 60427

DISTRIBUTION LIST

No. of Copies	Organization
2	McDonnell-Douglas Astronautics Company 5301 Bolsa Avenue ATTN: Dr. L. B. Greszczuk Dr. J. Wall Huntington Beach, CA 92647
1	New Mexico Institute of Mining and Technology ATTN: TERA Group Socorro, NM 87801
1	Northrup Corporation 3901 W. Broadway ATTN: R. L. Ramkumar Hawthorne, CA 90250
1	Nuclear Assurance Corporation 24 Executive Park West ATTN: T. C. Thompson Atlanta, GA 30245
1	Pacific Technical Corporation 460 Ward Drive ATTN: Dr. F. K. Feldmann Santa Barbara, CA 93105
2	Schumberger Well Services Perforating Center ATTN: J. E. Brooks J. Brookman PO Box A Rosharon, TX 77543
1	Science Applications, Inc. 101 Continental Boulevard Suite 310 El Segundo, CA 90245
1	Ship Systems, Inc. 11750 Sorrento Valley Road ATTN: Dr. G. G. Erickson San Diego, CA 92121
1	Systems, Science and Software PO Box 1620 ATTN: Dr. R. Sedgwick La Jolla, CA 92038
2	TRW One Space Park, R1/2120 ATTN: D. Ausherman M. Bronstein Redondo Beach, CA 90277
1	United Technologies Research Center 438 Weir Street ATTN: P. R. Fitzpatrick Glastonbury, CT 06033
1	US Steel Corporation Research Center 125 Jamison Lane Monroeville, PA 15146
1	VPI & SU 106C Norris Hall ATTN: Dr. M. P. Kamat Blacksburg, VA 24061
2	Vought Corporation PO Box 225907 ATTN: Dr. G. Hough Dr. Paul M. Kenner Dallas, TX 75265
1	Westinghouse, Inc. PO Box 79 ATTN: J. Y. Fan W. Mifflin, PA 15122
1	Drexel University Department of Mechanical Engr. ATTN: Dr. P. C. Chou 32d and Chestnut Streets Philadelphia, PA 19104

DISTRIBUTION LIST

No. of Copies	Organization
1	Forrestal Research Center Aeronautical Eng. Laboratory Princeton University ATTN: Dr. A. Eringen Princeton, NJ 08540
3	Southwest Research Institute Dept. of Mechanical Sciences ATTN: Dr. U. Lindholm Dr. W. Baker Dr. R. White 8500 Culebra Road San Antonio, TX 78228
4	SRI International 333 Ravenswood Avenue ATTN: Dr. L. Seaman Dr. L. Curran Dr. D. Shockey Dr. A. L. Florence Menlo Park, CA 94025
1	State University of New York at Stony Brook Department of Materials Science and Engineering ATTN: Dr. H. Herman Stony Brook, NY 11790
2	University of Arizona Civil Engineering Department ATTN: Dr. D. A. DaDeppo Dr. R. Richard Tucson, AZ 85721
1	University of Arizona School of Engineering ATTN: Dean R. Gallagher Tucson, AZ 85721
1	University of California Los Angeles ATTN: Dr. M. Ziv Los Angeles, CA 90024
1	University of California Department of Physics ATTN: Dr. Harold Lewis Santa Barbara, CA 93106
2	University of California College of Engineering ATTN: Prof. W. Goldsmith Dr. A. G. Evans Berkeley, CA 94720
2	University of Delaware Department of Mechanical Engineering ATTN: Prof. J. Vinson Prof. B. Pipes Newark, DE 19711
1	University of Denver Denver Research Institute ATTN: Mr. R. F. Recht 2390 S. University Blvd. Denver, CO 80210
2	University of Florida Department of Engineering Sciences ATTN: Dr. R. L. Sierakowski Dr. L. E. Malvern Gainesville, FL 32601
1	University of Oklahoma School of Aerospace, Mechanical and Nuclear Engineering ATTN: Dr. C. W. Bert Norman, OK 73019
1	University of Vermont 201 Votey Bldg. ATTN: C. Brown Burlington, VT 05405

DISTRIBUTION LIST

No. of Copies	Organization	No. of Copies	Organization

Aberdeen Proving Ground

Dir, USAMSAA
ATTN: DRXSY-D
DRXSY-MP, H. Cohen
Cdr, USATECOM
ATTN: DRSTE-TO-F
Dir, USAAPG
ATTN: Mr. S. Keithely, MTD

Dir, USACSL, EA
ATTN: DRDAR-CLB-PA
Bldg. E3516

USER EVALUATION OF REPORT

Please take a few minutes to answer the questions below; tear out this sheet, fold as indicated, staple or tape closed, and place in the mail. Your comments will provide us with information for improving future reports.

1. BRL Report Number _____

2. Does this report satisfy a need? (Comment on purpose, related project, or other area of interest for which report will be used.)

_____

_____

_____

3. How, specifically, is the report being used? (Information source, design data or procedure, management procedure, source of ideas, etc.) _____

_____

_____

4. Has the information in this report led to any quantitative savings as far as man-hours/contract dollars saved, operating costs avoided, efficiencies achieved, etc.? If so, please elaborate.

_____

_____

5. General Comments (Indicate what you think should be changed to make this report and future reports of this type more responsive to your needs, more usable, improve readability, etc.) _____

_____

_____

_____

6. If you would like to be contacted by the personnel who prepared this report to raise specific questions or discuss the topic, please fill in the following information.

Name: _____

Telephone Number: _____

Organization Address: _____

_____

_____